Supplement of Biogeosciences, 12, 3469–3488, 2015
http://www.biogeosciences.net/12/3469/2015/
doi:10.5194/bg-12-3469-2015-supplement

Biogeosciences Open Access

Supplement of

Observation-based modelling of permafrost carbon fluxes with accounting for deep carbon deposits and thermokarst activity

T. Schneider von Deimling et al.

Correspondence to: T. Schneider von Deimling (thomas.schneider@awi.de)

1. Terminology and definitions

Active layer: The layer of ground that is subject to annual thawing and freezing in areas underlain by permafrost (van Everdingen, 2005)

Differentiation between Mineral Soils and Organic Soils:

> **Mineral soils:** Including mineral soil material (less than 2.0 mm in diameter) and contain less than 20 percent (by weight) organic carbon (Soil Survey Staff, 1999). Here including Orthels and Turbels (see definition below).
>
> **Organic soils:** Soils including a large amount of organic carbon (more than 20 percent by weight, Soil Survey Staff, 1999). Here including Histels (see definition below).

Gelisols: Soil order in the Soil taxonomy (Soil Survey Staff, 1999). Gelisols include soils of very cold climates, containing permafrost within the first 2m below surface. Gelisols are divided into 3 suborders:

> **Histels:** Including large amounts of organic carbon that commonly accumulate under anaerobic conditions (>80 vol % organic carbon from the soil surface to a depth of 50 cm) (Soil Survey Staff, 1999).
>
> **Turbels:** Gelisols that have one or more horizons with evidence of cryoturbation in the form of irregular, broken, or distorted horizon boundaries, involutions, the accumulation of organic matter on top of the permafrost, ice or sand wedges (Soil Survey Staff, 1999).
>
> **Orthels:** Gelisols that show little or no evidence of cryoturbation. These soils occur primarily within the zone of widespread permafrost. Orthels are generally drier than Turbels and Histels (Soil Survey Staff, 1999).

Near-surface and deep deposits: Following Hugelius et al. (2014), we define the boundary between near surface and deep deposits at 3 meters depth.

Peatland: Peat-covered terrain (according to van Everdingen, 2005). A peatland is a special type of wetland (see definition below) formed by the accumulation of plant remains. Peatlands contain more than 40 cm of peat accumulation on which organic soils develop (National Wetlands Working Group, 1988)

Taberit: Generalizing the definition by Kaplina (1981), who defined taberal deposits from a sedimentoligical and stratigraphical point of view, we use this term in the sense of the process of in-situ thawing under a large water body. Independently from the recent ground temperature (refrozen or non-frozen), we define taberal deposits as permafrost sediments that underwent thawing in a talik (see definition below), resulting in diagenetic alteration of sediment structures (i.e., loss of original cryostructure, sediment compaction) and biogeochemical characteristics (i.e., depletion of organic carbon under anaerobic conditions).

Talik: A layer or body of perennially unfrozen ground occurring in a permafrost area due to a local anomaly in thermal, hydrological, hydrogeological, or hydrochemical conditions. For example, a lake talik is caused by the heat storage effect of the lake water (according to van Everdingen, 2005).

Thermokarst (process): A process by which characteristic landforms, such as lakes or basins, result from the thawing of ice-rich permafrost and subsequent surface subsidence (van Everdingen, 2005).

Thermokarst deposits: Used according to Strauss et al. (2013) to describe the (re-)frozen deposits accumulated in drained thaw-lake basins and thermo-erosional valleys.

Wetland: A land that is saturated with water long enough to promote wetland or aquatic processes as indicated by poorly drained soils, hydrophytic (water-tolerant) vegetation, and various kinds of biological activity that are adapted to a wet environment (National Wetlands Working Group, 1988)

Yedoma: A suite of late Pleistocene ice- and organic-rich silty sediments that contain large syngenetic ice wedges and accumulated in Beringia (unglaciated Siberia and Alaska) (Schirrmeister et al., 2013).

Yedoma deposits: Used according to Strauss et al. (2013) to emphasize that the deposit itself (not the geomorphic or the stratigraphic position (Schirrmeister et al., 2013)) is meant. The studied recent Yedoma deposits are undisturbed and unaltered by thermokarst processes.

Yedoma region: We used this term to outline the potential area for Yedoma deposit distribution, not to indicate the area where Yedoma deposits indeed occur (Strauss et al., 2013). The occurrence of Yedoma deposits in the Yedoma region is fragmented by thermokarst and fluvial processes and thus also includes other types of deposits in addition to Yedoma deposits.

Hugelius, G., Strauss, J., Zubrzycki, S., Harden, J., Schuur, E. A. G., Ping, C.-L., Schirrmeister, L., Grosse, G., Michaelson, G., Koven, C., O'Donnel, J., Elberling, B., Mishra, U., Camill, P., Yu, Z., Palmtag, J., and Kuhry, P.: Improved estimates show large circumpolar stocks of permafrost carbon while quantifying substantial uncertainty ranges and identifying remaining data gaps, Biogeosciences Discussions, 11, 4771-4822, 10.5194/bgd-11-4771-2014, 2014.

National Wetlands Working Group (Tamocai, C., chairman) 1988. Wetlands of Canada. Ecological Land Classification Series, No. 24. Environment Canada and Polyscience Publications Inc. Ottawa, Ontario. 452 p. Schirrmeister, L., Froese, D. G., Tumskoy, V., Grosse, G., and Wetterich, S.: Yedoma: Late Pleistocene ice-rich syngenetic permafrost of Beringia, in: Encyclopedia of Quaternary Sciences, 2 ed., edited by: Elias, S. A., Elsevier, Amsterdam, 542-552, 2013.

Soil Survey Staff: Soil taxonomy: A basic system of soil classification for making and interpreting soil surveys, 2nd Edn., United States Department of Agriculture, Washington, 869 pp., 1999. Strauss, J., Schirrmeister, L., Grosse, G., Wetterich, S., Ulrich, M., Herzschuh, U., and Hubberten, H.-W.: The Deep Permafrost Carbon Pool of the Yedoma Region in Siberia and Alaska, Geophysical Research Letters, 40, 6165–6170, 10.1002/2013GL058088, 2013.

van Everdingen, R. O.: Multi-language glossary of permafrost and related ground-ice terms, National Snow and Ice Data Center, Boulder, USA, 2005.

2. Model description

2.1 Model initialization

Permafrost carbon inventory

Based on updated soil carbon data (Hugelius et al., 2013) we describe the amount of organic matter in near-surface permafrost which we allocate into a mineral soil pool (SOCC<20% per weight, 540 Pg-C) and into an organic soil pool (SOCC>20%, 120 Pg-C), separately for the depth levels 0 to 1m, 1 to 2m, and 2 to 3m. We hereby focus on carbon in permafrost-affected soils, i.e. orthels and turbels for the mineral pools, and histels for the organic pools (see Fig. 1). Furthermore, we consider two additional pools to describe carbon stored in ice-rich deep deposits ranging from the surface to a depth of 15m. Following the inventory classification by Strauss et al. (2013), we consider a Yedoma pool (~80 Pg-C, 0 to 15m) and a refrozen thermokarst pool (~130 Pg-C, 0 to 5m). To avoid double-accounting of near-surface inventory estimates, we subtract the amount of permafrost carbon in the top three meters of the Yedoma and refrozen thermokarst pools (Strauss et al., 2013) from the near-surface mineral soil pool (Hugelius et al., 2013). While the Yedoma pool classifies carbon deposits unaffected by past thermokarst activity, the refrozen thermokarst pool describes organic material buried in sediments which had been subject to abrupt permafrost thaw in the past. In addition to the estimate of Yedoma and thermokarst carbon deposits by Strauss et al. (2013), we also consider permafrost carbon stored in deep taberal sediments (~110 Pg-C, Walter-Anthony et al., 2014) in the depth range 5 to 15m (Fig.1). We do not separately consider an estimated 70 Pg-C stored perennially frozen in deep deltaic alluvium (Hugelius et al., 2014). The potential for intensive future thermokarst formation (and thus for deep thaw) in typical deltaic landscapes is rather small, thus we assume that a large portion of this deep carbon store will remain frozen over the next centuries.

As we start our simulations from pre-industrial climate, we enlarge our data-based near-surface carbon pools by 10%. This increase accounts for historical permafrost carbon release and matches the amount of simulated permafrost carbon at the year 2000 with the inventory estimates by Hugelius et al. (2014).

Permafrost temperatures and active layer profile

To fully initialize our model, we had to determine permafrost ground temperatures of our carbon inventory. Actual observations, however, are limited and we therefore make the simplifying assumption that ground temperatures are to first order determined by surface air temperatures. We used climatology data from the Berkeley Earth dataset (http://berkeleyearth.org/data) to partition our permafrost grid cells (which range from 47°N to

84°N) into bins of varying surface air temperatures[1]. Based on typical north-south gradients of mean annual ground temperatures (MAGTs) (Romanovsky et al., 2010;Beer et al., 2013), we assume that the bin with the warmest air temperatures corresponds to southern and warm permafrost with an initial MAGT of –0.5°C ($MAGT_{Max}$), and that the bin with coldest air temperatures corresponds to northern permafrost with an initial MAGT of –10°C ($MAGT_{Min}$). For our default parameter setting, we linearly scale the remainder of temperature bins between $MAGT_{Max}$ and $MAGT_{Min}$. To account for uncertainty, we use a non-linear scaling to allow for clustering towards warmer or colder initial MAGTs (with keeping the total range of –10 to –0.5°C fixed).

After initialization, MAGT is re-calculated at each time-step for each depth level between the soil surface and the active layer depth. Hereby we assume that soil temperatures equilibrate instantaneously to changing surface air temperatures at the soil surface, while deeper soil layers reveal a time lagged response. The vertical soil temperature profile can be inferred from the condition that maximum summer temperatures equal zero degrees Celsius at the active layer depth. Soil temperatures *TS(t)* between the surface and the active layer depth are scaled such that time lag increases linearly with depth.

We determine the latitudinal profile of the active layer based on our prescribed north-south gradient of initial MAGTs. We assume the seasonal ground temperature cycle to exponentially decay with depth and we choose a typical scale depth to infer temperature profiles consistent with observed, "trumpet-shaped" soil temperature profiles (Romanovsky et al., 2010;Boike et al., 2013).We then define the equilibrium active layer level for each soil pool and for each latitude as the depth at which maximum soil summer temperatures equal zero degrees. Warmer locations or stronger seasonal cycles result in deeper active layers than colder regions or locations of reduced annual temperature ranges (see Koven et al. (2013)).

2.2 Thaw rate parametrization

We model the process of long-term active layer deepening by assuming that thaw rates can be parametrized depending on four key factors: thermal ground properties, mean annual ground temperatures, active layer depth, and magnitude of the regional warming anomaly which drives permafrost degradation. For each latitudinal band *lat*, soil type *S*, and aerobic/anaerobic regime *A*, we separately calculate the time evolution of active layer depths by describing individual thaw rates $TR(t)$:

[1] We use summer air temperatures because they are likely to result in a better representation of the soil thermal state compared to annual mean air temperatures. Cold winter air temperatures do not fully penetrate into the ground because snow cover is an effective thermal insulator.

$$TR(t)_{S,A,lat} = \alpha_{S,A} * S(t)_{S,A,lat} * \frac{dT^*(t)_{A,lat}}{z_{ALD}(t)_{S,A,lat}} \quad (1),$$

with α describing aggregated soil-specific thermal diffusivities, $S(t)$ a soil temperature dependent scaling, $dT^*(t)$ the thaw driving surface warming anomaly, and $z_{ALD}(t)$ the active layer depth. The choice for these four factors is motivated in the following:

1) $\alpha_{S,A}$ is a soil-specific parameter (*aggregated thermal diffusivity*) which determines how effectively heat can penetrate into the ground. Hereby we assume that heat diffusion into the frozen ground is to first order determined by the ice content of the sediments. We first prescribe α_S for mineral soils under aerobic conditions and then use scaling factors to infer thermal diffusivities for the remaining carbon pools. As the high latent heat content of ice-rich deposits impedes the rate of downward thawing (Jorgenson et al., 2010), we scale α_S according to assumed ice contents (typical mineral soils: 25 vol%, Yedoma: 70 vol%, refrozen thermokarst: 45 vol% (Schirrmeister et al., 2011;Strauss et al., 2013). For organic soils we assume a reduced thermal diffusivity compared to mineral soils (factor 0.5) given higher ice contents and the low thermal conductivity of organic matter. When lakes grow deep enough to prevent winter refreeze, permafrost degradation increases substantially due to year-round thawing (Arp et al., 2012). To capture the increase in thaw rates after thermokarst formation, we tune $\alpha_{S,A}$ to match simulated talik propagation of Kessler et al. (2012). If soils are subject to wetland conditions (i.e. they are moisture-saturated but are not covered by lakes), we assume a reduced thermal diffusivity given the higher ice contents in these soils (see Table 1).

2) When permafrost is close to zero degrees Celsius, almost all heat is used for the phase transition from ice to water, while for colder conditions the majority of the warming anomaly is used to increase permafrost temperatures with little downward propagation of the thaw front. To capture the difference between much lower thaw rates in cold as compared to warm permafrost (see Schaphoff et al. (2013), we describe a latitude-dependent scaling factor $S(t)_{lat}$ which non-linearly scales thaw rates by mean annual ground temperatures (MAGTs). Hereby, we describe a quartic dependency of $S(t)_{lat}$ on MAGT to capture the sharp increase in thaw rates when permafrost temperatures approach zero degrees Celsius. The scaling factor profile is parametrized to yield a ratio of 1:10 for thaw rates at coldest (MAGT= –10°C) to warmest (MAGT=0°C) permafrost.

3) We capture the strong dampening of heat propagation with depth by assuming that the thaw rate is inversely proportional to depth (Kessler et al., 2012). This allows us to reproduce the general tendency of high talik development rates in the first years after thermokarst initiation and gradual decrease with time (Ling, 2003).

4) The magnitude of the regional surface warming anomaly is a further key driver of subsurface permafrost degradation. We assume thaw rates in non-thermokarst affected sediments being proportional to the magnitude of the surface air temperature anomaly, i.e. the warming above pre-industrial temperatures. We calculate the warming anomaly in each latitudinal band by accounting for the length of the thaw season (i.e. by the yearly fraction of days with non-freezing surface air temperatures). To account for key differences in thaw rates between non-thermokarst and thermokarst-affected sediments, we assume that degradation of the latter is driven over a full year by lake bottom temperatures (and thus not by seasonal surface air temperatures). We calculate lake bottom temperatures based on the annual cycle of surface air temperatures while assuming that the annual summer amplitude is damped by 50% (Boike et al., 2013) and that winter lake bottom temperatures cannot fall below a minimum of two degrees Celsius.

To ensure that our scheme for describing permafrost thaw dynamics yields robust results, we perform a consistency check at each time step: we calculate the equilibrium active layer depth which would establish under the given climatic boundary conditions (determined by mean annual air temperature and the amplitude of the seasonal cycle). We use this depth as a constraint for maximum thaw rates and thus assure that the parametrization of thaw rates yields physically plausible results.

2.3 Anaerobic soil fractions

In our study, we assume that anaerobic soil fractions will not stay static under climate change. We hereby make differing assumptions of how anaerobic soil fractions (thermokarst lakes and wetlands) will evolve in a warmer climate (see section 3.1 and 3.2). In both cases, we assume that increases in anaerobic soil fractions will decrease the aerobic soil fraction, while a reduction of anaerobic soil fractions will increase the fraction of aerobic soils. We do not consider the case in which a thermokarst lake develops into a wetland by terrestrialization, or the reverse case of a wetland becoming a thermokarst-affected terrain.

Thermokarst lake pool

To capture future thermokarst dynamics, we have developed a conceptual model of thermokarst formation and drainage. Our simulation approach is chosen to test different hypotheses of future thermokarst evolution rather than providing a deterministic model projection based on small-scale thermokarst processes (such as e.g. Kessler et al. (2012), Ling et al. 2012). To keep our model description as simple as possible, we assume that future increases in surface air temperatures are the main driver for new thermokarst formation through melting of near-surface ground ice and subsequent ground subsidence. Moreover, we neglect factors

other than temperature (e.g. surface disturbance, precipitation or local topography) which also can affect thermokarst formation (van Huissteden et al., 2011).

To describe the evolution of newly formed thermokarst lakes in each latitudinal band, we use an optimum function which non-linearly scales the latitudinal thermokarst lake area fraction $F^{TKL}(t)$ by the surface air temperature anomaly $dT'(t)$ (see Fig. S1):

$$F^{TKL}{}_{S,lat}(t) = d_S * \exp(a_S * dT'(t) - b_S * dT'(t)^{c_{lat} * dT'(t)}) \quad (2)$$

For each soil pool $F^{TKL}(t)$ describes the area fraction per latitudinal band which is affected by newly formed thermokarst lakes. The high-latitude surface air temperature anomaly $dT'(t)$ drives changes in thermokarst lake extent. It is defined as the annual surface air warming above pre-industrial temperatures, averaged over all permafrost regions. We infer $dT'(t)$ based on an analysis of polar amplification factors from state-of-the-art climate models (CMIP-5, (Taylor et al., 2011). With rising $dT'(t)$, $F^{TKL}(t)$ increases towards an optimum at which the maximum thermokarst lake fraction F^{TKLmax} is realized at dT'^{TKLmax}. With further warming above dT'^{TKLmax} drainage and additional processes (such as increasing evaporation and terrestrialization (van Huissteden and Dolman, 2012) are assumed to outweigh lake formation. By our model design, further warming above dT'^{TKLmax} leads to a decrease in the thermokarst lake area which cannot fall below a prescribed minimum area fraction F^{TKLmin}. We prescribe a decline which is most pronounced in southern permafrost regions where we assume a minimum fraction of remaining lakes F^{TKLmin} of 3% (see Fig. S1). In the coldest permafrost regions we assume a minimum fraction of 15%. The latitudinal gradient expresses the potential for more extensive drainage at the southern, discontinuous permafrost boundary where the permafrost body is thin and where internal drainage (i.e. subterraneous outflow (Yoshikawa and Hinzman, 2003)) is an efficient pathway for water removal. In northern, continuous permafrost regions, we only consider lateral erosion through thermo-erosional landforms and expansion of lakes in thermokarst basins (Morgenstern et al., 2011) an efficient drainage mechanism. We determine the soil-specific shape parameters a_S, b_S, d_S by prescribing F^{TKLmax} and $dT'(t)$ for each carbon pool individually (see Table 1).

In specific regions, about 80% of the landscape is affected by thermokarst and thermal erosion (Strauss et al., 2013). Yet it is unlikely that future thermokarst coverage will be as extensive because existing degradational landforms and other topographic lows will favour future lake drainage (Morgenstern et al. 2011). We assume the highest potential for new thermokarst lake formation in unaltered ice-rich Yedoma deposits which had not been affected by past thermokarst activity. We further assume a reduced potential for the formation of second-generation lakes in existing basins (Morgenstern et al. 2011), i.e. in refrozen thermokarst

deposits. The lowest potential of new thermokarst lake formation is assumed for less ice-rich organic and mineral soils (see Table 1).

By newly formed lakes we consider thermokarst lakes which establish under temperatures warmer than pre-industrial. We do not consider existing thermokarst lakes (formed over the last centuries to millennia) as a part of our thermokarst lake pool. These lakes have likely formed deep taliks in the past and are underlain by sediments potentially depleted in labile organic matter. We further only consider lakes being part of our thermokarst pool if they are deep enough to prevent winter refreeze of the lake bottom waters (about 1 to 2m (Arp et al., 2012;Yi et al., 2014)). As we do not model lake depth expansion we assume that formation of new thermokarst lakes is initiated for any warming above our reference climate (i.e. pre-industrial climate), while we also assume that extensive talik formation under thermokarst lakes is only realized after newly formed lakes have deepened enough to reach the critical depth which prevents winter refreeze (we define this time to be the year 2000). Arctic landscapes are also covered by numerous smaller lakes or ponds which fully refreeze in winter and do not develop deep taliks. Therefore they do not provide conditions for abrupt permafrost degradation and we consider ponds and smaller lakes part of our wetland pool.

We do not account for changes of the CO_2 and CH_4 flux balance through establishment of new vegetation after drainage (van Huissteden and Dolman, 2012; Kessler et al., 2012; Jones et al., 2012; Walter Anthony et al., 2014), see discussion in section model limitations).

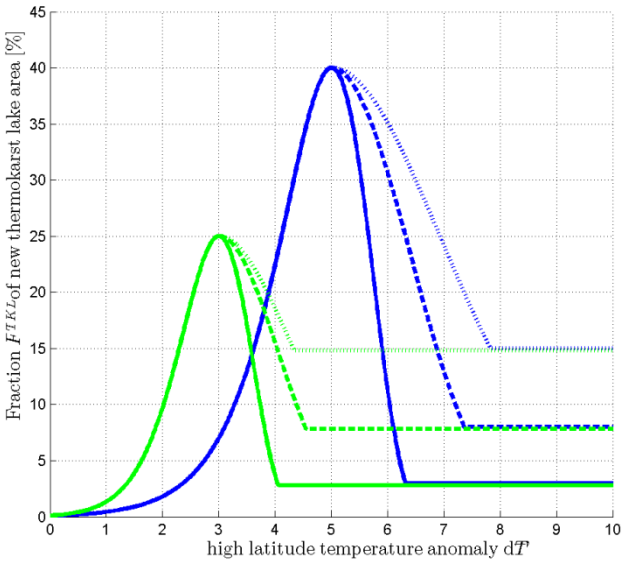

Fig.S1. Temperature dependency of newly formed thermokarst lake area fractions. The figure illustrates the increase and decrease of the new thermokarst lake area fraction F^{TKL} (as percentage of the total permafrost area in each latitudinal band) with rising high latitude surface air warming dT'. Curves are shown for two different choices of maximum thermokarst

lake extents $\mathrm{F}^{\mathrm{TKLmax}}$ (green: 25%, blue: 40%) and corresponding warming $\mathrm{dT'}^{\mathrm{TKLmax}}$ (green: 3°C, blue: 5°C). The different line styles illustrate the latitudinal dependency of drainage for warming above $\mathrm{dT'}^{\mathrm{TKLmax}}$ (solid: southern permafrost limit, dashed: mid permafrost latitude, dotted: northern permafrost limit).

Wetland pool

In this study we assume that high latitude wetland extent will slightly increase over the near-term with future warming. Such an assumption is supported by projected increases in the hydrologic balance of precipitation minus evaporation (AICA, Wash et al., chapter 6, 2009). We do not investigate a scenario of potential northern wetland drying (as e.g. investigated by Avis et al. (2011)). In our model setting we describe an increase in the wetland area fraction per latitudinal band by a linear scaling with high latitude warming, i.e. with the high-latitude surface air temperature anomaly $\mathrm{dT'(t)}$. Each carbon pool is initialized with a minimum wetland extent at pre-industrial temperatures and reaches its maximum extent for a high-latitude warming $\mathrm{dT'}$ of 10°C (see Table 1). For further warming the wetland fraction is kept constant at the maximum extent.

Our simulated wetland CH_4 fluxes describe CH_4 produced from newly thawed permafrost carbon. Yet the full carbon balance of wetlands is rather complex and possibly more affected by future changes in soil moisture, soil temperature, and vegetation composition than by the delivery of newly thawed organic matter through permafrost degradation (Olefeldt et al., 2013). The accounting of these additional factors requires the implementation of comprehensive wetland models (such as formulated by Kleinen et al. (2012) and Frolking et al. (2001)).

2.4 Carbon release

Based on our thaw rate parametrization (equation 1), we track the active layer depth for each pool at each time step and thus can calculate the amount of carbon which is thawed as a consequence of warming above pre-industrial temperatures. We refer to this newly thawed carbon as vulnerable carbon VC(t) (Burke et al., 2012). Carbon release $C^{\uparrow}(t)$ for each soil carbon pool S, aerobic/anaerobic environment A, organic matter quality Q, latitude lat, and depth level z is assumed proportional to the pool-specific amount of vulnerable carbon $VC(t)$ and release rate R(t) (see Table 1):

$$C^{\uparrow}{}_{S,A,Q,lat,z}(t) = R_{S,A,Q,lat,z}(t) * VC_{S,A,Q,lat,z}(t) \quad (3)$$

We do not explicitly account for gaseous transport from subsoil layers to the atmosphere but assume that the timescale involved is small compared to CO_2 and CH_4 production. Therefore, we assume that carbon release rates can be described by CO_2 and CH_4 production rates. Yet we account for pool-specific oxidation during CH_4 release. We hereby assume little oxidation of CH_4 from thermokarst sediments because ebullition is a rather effective pathway with little chance for CH_4 oxidation. To the contrary, CH_4 release from wetlands is likely affected much stronger by oxidation. We therefore assume systematically higher oxidation rates for these soils (see Table 1).

Under anaerobic degradation of organic matter, CH_4 can be produced via a variety of complex food webs (Segers, 1998). For our fast pool (which describes labile organic matter) we assume that CH_4 production is dominated by fermentation of acetate. Given the stoichiometry of CH_4 production by methanogenesis via this pathway, we assume a 1:1 production ratio of CH_4:$CO_2^{anaerobic}$ (Walter Anthony et al., 2014;Conrad et al., 2002). Incubations studies suggest this ratio can deviate strongly from 1:1 and cover very large ranges with anaerobic CO_2 production one to two orders of magnitude larger than CH_4 production (Lee et al., 2012;Scanlon and Moore, 2000;Segers, 1998). We do not account for very low CH_4:$CO_2^{anaerobic}$ ratios (<0.07) which might be explained by high initial CO_2 production and a strong decline with time after which a stable, much larger CH_4:$CO_2^{anaerobic}$ ratio might establish (Scanlon and Moore, 2000).
Compared to the amount of labile organic matter, the slow carbon pools describe a much larger inventory of organic material of varying compositions and structures. We assume that CH_4 production can also follow alternative pathways under which alternative electron acceptors are likely becoming important which can reduce CH_4:$CO_2^{anaerobic}$ production ratios. Based on incubation results from Lee et al. (2013), we assume an anaerobic production ratio CH_4:$CO_2^{anaerobic}$ of 1:7 (±50%) for organic matter in the slow pool (Table 1).

As microbial soil activity rises with increasing soil temperatures, we account for a Q_{10} temperature sensitivity of carbon decomposition: we calculate carbon release rates R(t) for each carbon pool, each latitude, and each vertical layer by scaling CO_2 and CH_4 production rates P by monthly soil temperatures $TS(t)$:

$$R_{S,A,Q,lat,z}(t) = (1 - OX_A) * (P_{A,Q} * Q_A^{10^{(TS_{S,A,lat,z}(t)-10)/10}}) \quad (4)$$

We calculate monthly soil temperature *TS(t)* by assuming an exponential decay of the seasonal temperature cycle with depth. We hereby assume a lagged temperature response with time (i.e. zero lag at the soil surface which is assumed to warm at the same rate as surface air and maximum lag at the active layer depth). When soil temperatures drop below zero degrees Celsius we assume soil microbial activity to be negligible and decomposition is halted. $(1 -$

OX_A) describes the fraction of released carbon which is not oxidized (with $OX = 0$ for CO_2, and $OX = OX_{WET}$ or $OX = OX_{TKL}$ for CH_4, see Table 1).

2.5 Carbon-cycle and climate model

To close the feedback loop of warming-induced permafrost degradation, carbon release, and additional warming, we use a simple multi-box carbon-cycle climate model from Allen et al. (2009) which was designed to span the full range of temperature and carbon cycling dynamics consistent with observations.

The model calculates atmospheric CO_2 concentrations by describing a diffusive uptake of emitted CO_2 through vegetation and surface oceans, and by an advective carbon transport into the deep ocean. The uptake of heat by the ocean is modelled by a diffusive process. We have used the model description by Allen et al. (2009) and have extended their model design by describing a declining diffusive CO_2 uptake with rising temperatures. The extended diffusive description allows us to model a decrease in airborne fractions with rising temperatures inferred from complex models (Friedlingstein et al., 2006). We have tuned model parameters such that we could reproduce individual CO_2 concentration pathways from the RCP database (www.iiasa.ac.at/web-apps/tnt/RcpDb, Meinshausen 2011) based on CO_2 emission trajectories of all four standard RCPs. To calculate deviations in atmospheric CH_4 concentrations, we assume an exponential decay of CH_4 anomalies with a typical e-folding lifetime of 11 years.

We calculate radiative forcing of CO_2 and of CH_4 by using standard formulae after Myhre et al. (1998). Hereby, we also assume that indirect CH_4 effects lead to a radiative forcing which is about 15% larger than when only considering the direct radiative effect of changes in atmospheric CH_4 concentrations (Shindell et al., 2009). By describing uncertainty in the diffusive carbon uptake, in climate sensitivity, and in ocean heat uptake, our parameter sampling accounts for a large spread in simulated carbon-cycle climate responses. Based on the pathway of anthropogenic and permafrost-induced emission of CO_2 and CH_4, we thus can calculate the change in global mean surface air temperature (see also supplementary information in Allen et al. 2009).

As permafrost regions warm much stronger than the globe as a whole, it is important to account for the polar amplification of temperature change to simulate the warming of permafrost regions. We do this by applying latitude-dependent amplification factors which we infer from an analysis of state-of-the-art climate models (CMIP-5, (Taylor et al., 2011)). This analysis has resulted in typical amplification factors between 1.6 at the southernmost permafrost limit and about 2.3 at the northernmost permafrost limit. By using these scaling factors, we thus can translate our simulated global temperature anomalies into regional

warming of high-latitude permafrost regions. Based on these scaled temperatures anomalies, we calculate permafrost degradation in each latitudinal band.

3. Individual pool contributions and sensitivity runs

To illustrate how our individual soil carbon pools contribute to circumpolar carbon fluxes we show the contribution of all soil types and hydrologic fractions in figures S2 and S3. Further, we have performed two additional model simulations based on the same parameter sets where we run the model a) with stationary anaerobic fractions (i.e. with fixing wetland to initial extent and preventing formation of new thermokarst lakes), b) with neglecting the contribution of deep carbon deposits (see figure S4).

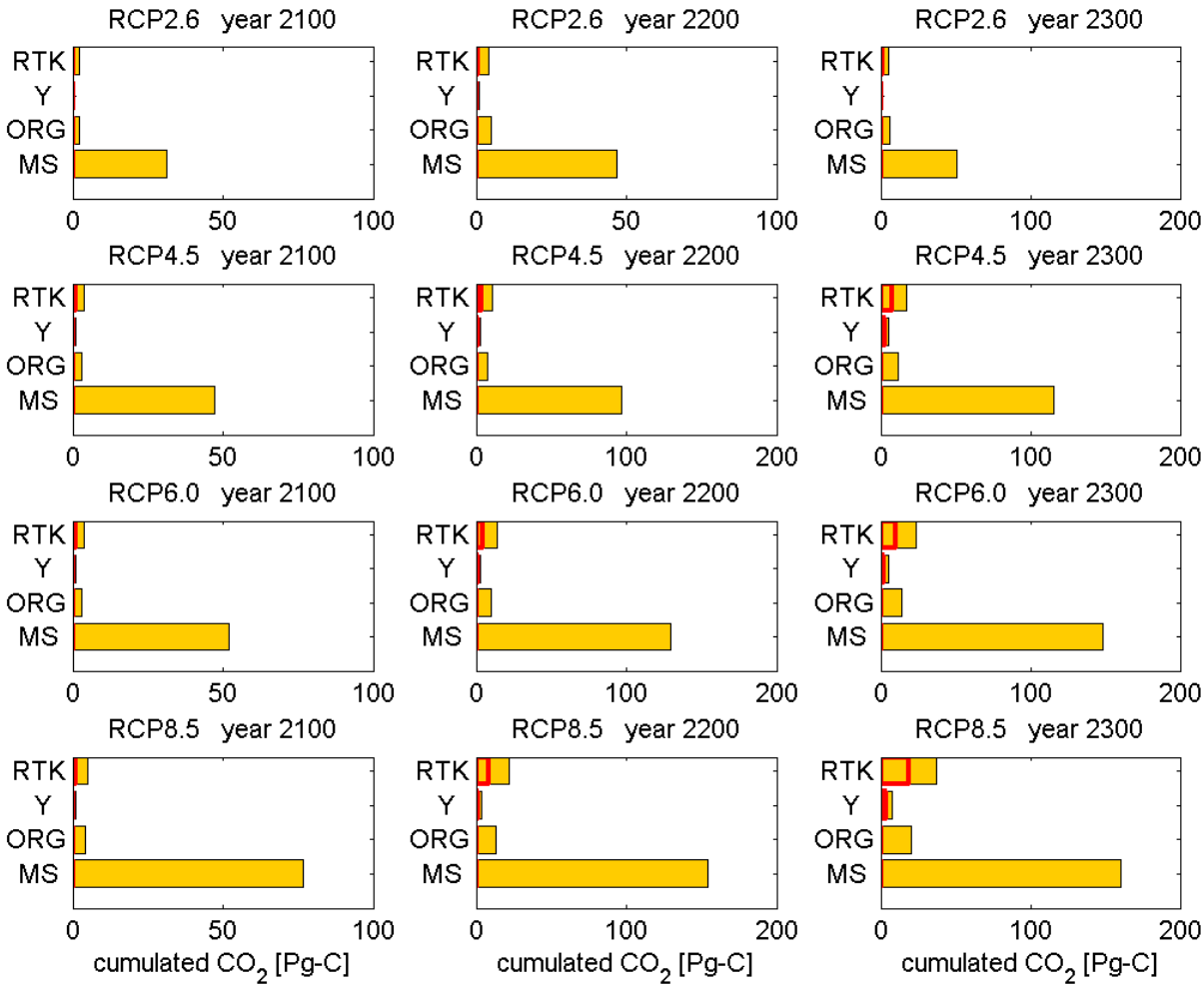

Fig. S2. Cumulated CO_2 fluxes from newly thawed permafrost for all soil types (MS: mineral, ORG: organic, Y: Yedoma, RTK: refrozen thermokarst) until the year 2100 (left column), until the year 2200 (middle column), and until the year 2300 (right column). Anthropogenic warming is increasing from top to bottom rows (RCP2.6 to RCP8.5). Red boxes illustrate the contribution of deep carbon deposits (below 3m depth). All contributions represent median estimates from a model ensemble of 500 runs which account for parameter uncertainty. Note the different x-axis scaling.

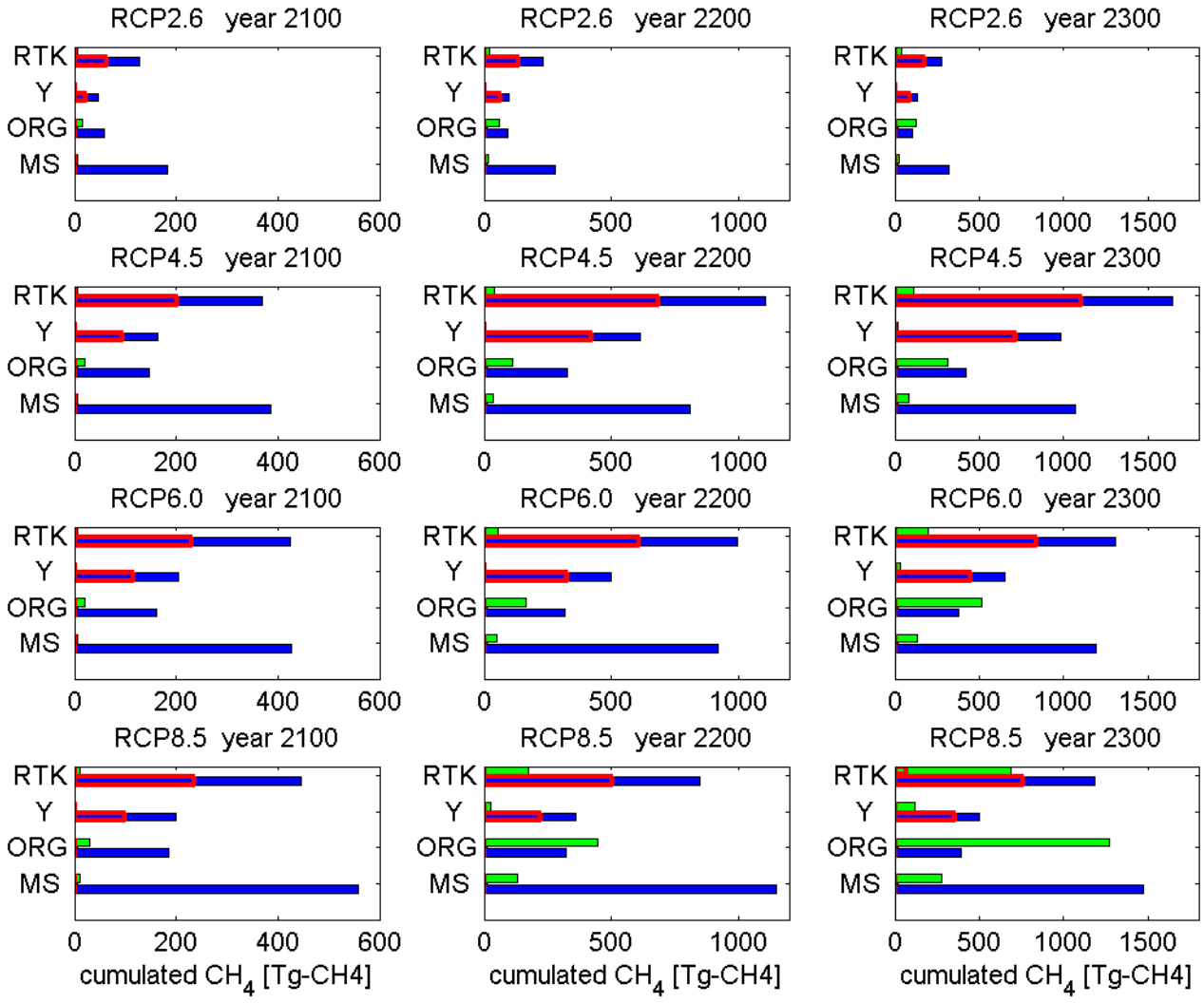

Fig. S3. Cumulated CH_4 fluxes from newly thawed permafrost for all soil types (MS: mineral, ORG:organic, Y: Yedoma, RTK: refrozen thermokarst) until the year 2100 (left column), until the year 2200 (middle column), and until the year 2300 (right column). Anthropogenic warming is increasing from top to bottom rows (RCP2.6 to RCP8.5). Blue bars describe the CH_4 contribution from newly formed thermokarst lakes, green bars describe the contribution from wetlands. Red boxes illustrate the contribution of deep carbon deposits (below 3m depth). All contributions represent median estimates of a model ensemble of 500 runs which account for parameter uncertainty. Note the different x-axis scaling.

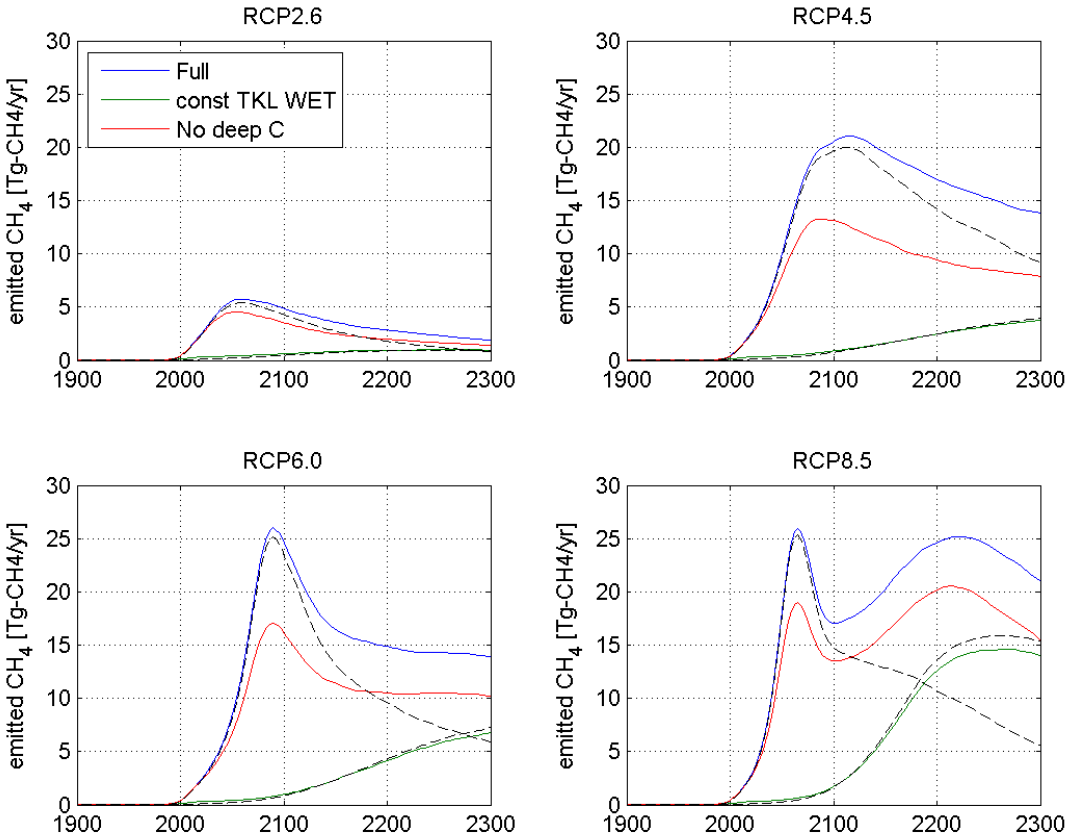

Fig. S4. Annual CH_4 release from newly thawed permafrost carbon under differing simulation settings: I) fluxes including contributions from changes in anaerobic fractions (wetlands and thermokarst) and accounting for deep deposits ("Full", blue lines), II) fluxes when keeping anaerobic fractions fixed at initial values ("const TKL WET", green lines), and III) fluxes without the contribution of deep deposits ("No deep C", red lines). Shown are median estimates from 500 member model ensembles. Black dashed lines illustrate the CH_4 contribution summed over all wetland and over all thermokarst lake pools.

Supplementary references

Arp, C. D., Jones, B. M., Lu, Z., and Whitman, M. S.: Shifting balance of thermokarst lake ice regimes across the Arctic Coastal Plain of northern Alaska, Geophysical Research Letters, 39, L16503, 10.1029/2012GL052518, 2012.

Avis, C. A., Weaver, A. J., and Meissner, K. J.: Reduction in areal extent of high-latitude wetlands in response to permafrost thaw, Nature Geosci, 4, 444-448, 2011.

Beer, C., Fedorov, A. N., and Torgovkin, Y.: Permafrost temperature and active-layer thickness of Yakutia with 0.5-degree spatial resolution for model evaluation, Earth Syst. Sci. Data, 5, 305-310, 10.5194/essd-5-305-2013, 2013.

Boike, J., Kattenstroth, B., Abramova, K., Bornemann, N., Chetverova, A., Fedorova, I., Fröb, K., Grigoriev, M., Grüber, M., Kutzbach, L., Langer, M., Minke, M., Muster, S., Piel, K., Pfeiffer, E. M., Stoof, G., Westermann, S., Wischnewski, K., Wille, C., and Hubberten, H. W.: Baseline characteristics of climate, permafrost and land cover from a new permafrost observatory in the Lena River Delta, Siberia (1998-2011), Biogeosciences, 10, 2105-2128, 10.5194/bg-10-2105-2013, 2013.

Conrad, R., Klose, M., and Claus, P.: Pathway of CH4 formation in anoxic rice field soil and rice roots determined by 13C-stable isotope fractionation, Chemosphere, 47, 797-806, 10.1016/S0045-6535(02)00120-0, 2002.

Friedlingstein, P., Cox, P., Betts, R., Bopp, L., von Bloh, W., Brovkin, V., Cadule, P., Doney, S., Eby, M., Fung, I., Bala, G., John, J., Jones, C., Joos, F., Kato, T., Kawamiya, M., Knorr, W., Lindsay, K., Matthews, H. D., Raddatz, T., Rayner, P., Reick, C., Roeckner, E., Schnitzler, K.-G., Schnur, R., Strassmann, K., Weaver, K., Yoshikawa, C., and Zeng, N.: Climate–Carbon Cycle Feedback Analysis: Results from the C4MIP Model Intercomparison, Journal of Climate, 19, 3337-3353, 10.1175/JCLI3800.1, 2006.

Frolking, S., Roulet, N. T., Moore, T. R., Richard, P. J. H., Lavoie, M., and Muller, S. D.: Modeling northern peatland decomposition and peat accumulation, Ecosystems, 4, 479-498, 2001.

Hugelius, G., Tarnocai, C., Broll, G., Canadell, J. G., Kuhry, P., and Swanson, D. K.: The Northern Circumpolar Soil Carbon Database: spatially distributed datasets of soil coverage and soil carbon storage in the northern permafrost regions, Earth Syst. Sci. Data, 5, 3-13, 10.5194/essd-5-3-2013, 2013.

Jones, M. C., Grosse, G., Jones, B. M., and Walter Anthony, K.: Peat accumulation in drained thermokarst lake basins in continuous, ice-rich permafrost, northern Seward Peninsula, Alaska, Journal of Geophysical Research: Biogeosciences, 117, G00M07, 10.1029/2011JG001766, 2012.

Jorgenson, M. T., Romanovsky, V., Harden, J., Shur, Y., O'Donnell, J., Schuur, E. A. G., Kanevskiy, M., and Marchenko, S.: Resilience and vulnerability of permafrost to climate change, Canadian Journal of Forest Research-Revue Canadienne De Recherche Forestiere, 40, 1219-1236, 2010.

Kessler, M. A., Plug, L. J., and Walter Anthony, K. M.: Simulating the decadal- to millennial-scale dynamics of morphology and sequestered carbon mobilization of two thermokarst lakes in NW Alaska, Journal of Geophysical Research: Biogeosciences, 117, G00M06, 10.1029/2011JG001796, 2012.

Kleinen, T., Brovkin, V., and Schuldt, R. J.: A dynamic model of wetland extent and peat accumulation: results for the Holocene, Biogeosciences, 9, 235-248, 10.5194/bg-9-235-2012, 2012.

Koven, C. D., Riley, W. J., and Stern, A.: Analysis of Permafrost Thermal Dynamics and Response to Climate Change in the CMIP5 Earth System Models, Journal of Climate, 26, 1877-1900, 10.1175/JCLI-D-12-00228.1, 2013.

Lee, H., Schuur, E. A. G., Inglett, K. S., Lavoie, M., and Chanton, J. P.: The rate of permafrost carbon release under aerobic and anaerobic conditions and its potential effects on climate, Global Change Biology, 18, 515-527, 10.1111/j.1365-2486.2011.02519.x, 2012.

Ling, F.: Numerical simulation of permafrost thermal regime and talik development under shallow thaw lakes on the Alaskan Arctic Coastal Plain, Journal of Geophysical Research, 108, 4511-4511, 2003.

Morgenstern, A., Grosse, G., Günther, F., Fedorova, I., and Schirrmeister, L.: Spatial analyses of thermokarst lakes and basins in Yedoma landscapes of the Lena Delta, The Cryosphere, 5, 849-867, 10.5194/tc-5-849-2011, 2011.
Myhre, G., Highwood, E. J., Shine, K. P., and Stordal, F.: New estimates of radiative forcing due to well mixed greenhouse gases, Geophys. Res. Lett., 25, 2715-2718, 1998.
Olefeldt, D., Turetsky, M. R., Crill, P. M., and McGuire, A. D.: Environmental and physical controls on northern terrestrial CH_4 emissions across permafrost zones, Global Change Biology, 19, 589-603, 10.1111/gcb.12071, 2013.
Romanovsky, V. E., Smith, S. L., and Christiansen, H. H.: Permafrost thermal state in the polar Northern Hemisphere during the international polar year 2007–2009: a synthesis, Permafrost and Periglacial Processes, 21, 106-116, 10.1002/ppp.689, 2010.
Scanlon, D., and Moore, T.: Carbon dioxide production from peatland soil profiles: The influence of temperature, oxic/anoxic conditions and substrate, Soil Science, 165, 153-160, 2000.
Schaphoff, S., Heyder, U., Ostberg, S., Gerten, D., Heinke, J., and Lucht, W.: Contribution of permafrost soils to the global carbon budget, Environmental Research Letters, 8, 014026, 2013.
Schirrmeister, L., Grosse, G., Wetterich, S., Overduin, P. P., Strauss, J., Schuur, E. A. G., and Hubberten, H.-W.: Fossil organic matter characteristics in permafrost deposits of the northeast Siberian Arctic, Journal of Geophysical Research: Biogeosciences, 116, G00M02, 10.1029/2011JG001647, 2011.
Segers, R.: Methane production and CH_4 consumption: a review of processes underlying wetland CH_4 fluxes, Biogeochemistry, 41, 23-51, 1998.
Shindell, D. T., Faluvegi, G., Koch, D. M., Schmidt, G. A., Unger, N., and Bauer, S. E.: Improved Attribution of Climate Forcing to Emissions, Science, 326, 716-718, 10.1126/science.1174760, 2009.
Strauss, J., Schirrmeister, L., Grosse, G., Wetterich, S., Ulrich, M., Herzschuh, U., and Hubberten, H.-W.: The deep permafrost carbon pool of the Yedoma region in Siberia and Alaska, Geophysical Research Letters, 40, 2013GL058088, 10.1002/2013GL058088, 2013.
Taylor, K. E., Stouffer, R. J., and Meehl, G. A.: An Overview of CMIP5 and the Experiment Design, Bulletin of the American Meteorological Society, 93, 485-498, 10.1175/BAMS-D-11-00094.1, 2011.
van Huissteden, J., and Dolman, A.: Soil carbon in the Arctic and the permafrost carbon feedback, Current Opinion in Environmental Sustainability, 4, 545-551, 2012.
Walter Anthony, K. M., Zimov, S. A., Grosse, G., Jones, M. C., Anthony, P. M., Iii, F. S. C., Finlay, J. C., Mack, M. C., Davydov, S., Frenzel, P., and Frolking, S.: A shift of thermokarst lakes from carbon sources to sinks during the Holocene epoch, Nature, 511, 452-456, 10.1038/nature13560, 2014.
Yi, S., Wischnewski, K., Langer, M., Muster, S., and Boike, J.: Freeze/thaw processes in complex permafrost landscapes of northern Siberia simulated using the TEM ecosystem model: impact of thermokarst ponds and lakes, Geosci. Model Dev., 7, 1671-1689, 10.5194/gmd-7-1671-2014, 2014.
Yoshikawa, K., and Hinzman, L. D.: Shrinking thermokarst ponds and groundwater dynamics in discontinuous permafrost near council, Alaska, Permafrost and Periglacial Processes, 14, 151-160, 10.1002/ppp.451, 2003.